

Cite this: *Chem. Sci.*, 2023, 14, 4605

All publication charges for this article have been paid for by the Royal Society of Chemistry

# Formation and fine-tuning of metal–organic frameworks with carboxylic pincers for the recognition of a C<sub>2</sub>H<sub>2</sub> tetramer and highly selective separation of C<sub>2</sub>H<sub>2</sub>/C<sub>2</sub>H<sub>4</sub>†

Yuefeng Duan,<sup>‡a</sup> Yuhang Huang,<sup>‡a</sup> Chongqing Wang,<sup>a</sup> Qian Wang,<sup>b</sup> Kai Ge,<sup>a</sup> Zhiyong Lu,<sup>ib</sup> Huijie Wang,<sup>a</sup> Jingui Duan,<sup>id</sup>\*<sup>a</sup> Junfeng Bai\*<sup>b</sup> and Wanqin Jin<sup>id</sup><sup>a</sup>

Highly efficient ethylene (C<sub>2</sub>H<sub>4</sub>) and acetylene (C<sub>2</sub>H<sub>2</sub>) separation is a great challenge and an important process in current industries. Herein, we finely tune a new family of 6-c metal–organic frameworks (MOFs) with crab-like carboxylic pincers for the recognition of a C<sub>2</sub>H<sub>2</sub> tetramer and afford NTU-72 with high adsorption C<sub>2</sub>H<sub>2</sub>/C<sub>2</sub>H<sub>4</sub> selectivity (56–441, 298 K) as well as unprecedented recovery of both highly pure C<sub>2</sub>H<sub>4</sub> (99.95%) and C<sub>2</sub>H<sub>2</sub> (99.36%). Furthermore, the effective binding of a C<sub>2</sub>H<sub>2</sub> tetramer by NTU-72's carboxylic pincers has been revealed by gas-loaded crystallography and Raman spectral studies. Our work provides a novel approach for the selective binding of a small molecular cluster for designing high-performance MOFs.

Received 16th February 2023

Accepted 2nd April 2023

DOI: 10.1039/d3sc00877k

rsc.li/chemical-science

## Introduction

As components of cracked gas, C<sub>2</sub>H<sub>4</sub> and C<sub>2</sub>H<sub>2</sub> are important raw materials for the synthesis of various organic compounds such as polyethylene,  $\alpha$ -ethynyl alcohols, and acrylic acid derivatives.<sup>1–3</sup> The preparation of these value-added products generally requires a high-purity feed gas. In industry, pure C<sub>2</sub>H<sub>4</sub> is realized by solvent absorption or selective catalytic hydrogenation from cracked gas, which are energy consuming processes.<sup>4,5</sup> Meanwhile, the recovery of high-purity C<sub>2</sub>H<sub>2</sub> is generally ignored in this process.

Adsorptive separation using porous materials is more environmentally friendly and energy efficient, and is regarded as a promising future separation technology.<sup>6–11</sup> As emerging porous materials, metal–organic frameworks (MOFs), derived from the self-assembly of organic ligands and inorganic nodes, demonstrate great opportunities to distinguish these two kinds of gas molecules by dedicated framework regulations, despite them having nearly identical molecular dimensions and physical properties.<sup>12–15</sup> For example, the MOF materials SIFSIX-Cu-i<sup>7</sup>

and NKMOF-1-Ni<sup>16</sup> exhibit minimal trade-off between adsorption capacity and selectivity, while the flexible UTSA-300 (ref. 17) demonstrates gating separation of these mixtures. However, they all produce lower purity C<sub>2</sub>H<sub>2</sub> during desorption, even for the sieving materials, as both C<sub>2</sub>H<sub>2</sub> and C<sub>2</sub>H<sub>4</sub> molecules can interact with strong binding sites, or the more or less flexibility of the sieving frameworks allows a certain amount of co-adsorption.<sup>18,19</sup>

MOFs with free carboxylic acids might be potential light hydrocarbon separation materials due to their remarkable characteristics of being a hydrogen bonding acceptor (O–H) and donor (C=O).<sup>20,21</sup> However, these MOFs have never been systematically investigated or intentionally designed for high-performance gas separation,<sup>22–24</sup> due to the significant coordination activity of carboxylic acids in MOF construction. We are interested in finely tuning MOFs to achieve efficient gas separations.<sup>25–28</sup> Herein, evolved from the interpenetrated **dia** topology,<sup>29</sup> a new family of 6-c MOFs (termed NTU-71 to NTU-73) with carboxylic pincers were designed based upon a C<sub>2v</sub> symmetric ligand of 3,5-di(1*H*-imidazol-1-yl)benzoic acid (**HL**) and the hybrid ions with different radii (SiF<sub>6</sub><sup>2–</sup> (*d*<sub>Si–F</sub>: 1.690 Å), TiF<sub>6</sub><sup>2–</sup> (*d*<sub>Ti–F</sub>: 1.886 Å) and ZrF<sub>6</sub><sup>2–</sup> (*d*<sub>Zr–F</sub>: 1.983 Å)). Among them, the distance of their carboxylic pincers has been finely tailored, and thus, they may approach those found in crab-like systems (Scheme 1). Very interestingly, NTU-72 exhibits a high C<sub>2</sub>H<sub>2</sub>/C<sub>2</sub>H<sub>4</sub> selectivity and great ability for recovery of both highly pure C<sub>2</sub>H<sub>4</sub> (99.95%) and C<sub>2</sub>H<sub>2</sub> (99.36%). This excellent separation performance is due to the stabilization of a C<sub>2</sub>H<sub>2</sub> tetramer by a couple of carboxylic pincers in the optimized pore geometry and size in NTU-72.

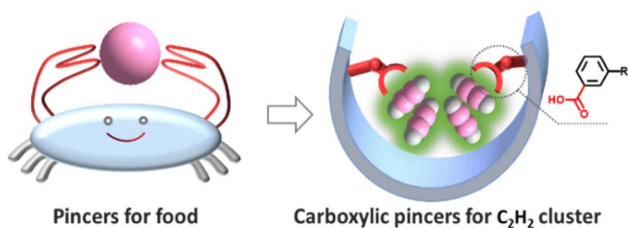
<sup>a</sup>State Key Laboratory of Materials-Oriented Chemical Engineering, Nanjing Tech University, Nanjing 211816, China. E-mail: duanjingui@njtech.edu.cn

<sup>b</sup>School of Chemistry and Molecular Engineering, Nanjing Tech University, Nanjing 211816, China. E-mail: hjunfeng@njtech.edu.cn

† Electronic supplementary information (ESI) available: Synthesis and characterization of these three crystals, PXRD, TGA, IR, sorption isotherms, IAST, breakthrough experiments and fitting parameters. CCDC 2211444–2211448, 2251139. For ESI and crystallographic data in CIF or other electronic format see DOI: <https://doi.org/10.1039/d3sc00877k>

‡ These authors contributed equally to this work.





Scheme 1 Crab-inspired MOF design incorporating carboxylic pincers for selective recognition of a  $C_2H_2$  cluster.

## Experimental section

General procedures of the experiment and simulation are available in the ESI.†

### Synthesis of NTU-70 to NTU-73

**Synthesis of NTU-71.** **HL** (4 mg, 0.015 mmol),  $CuSiF_6$  (10 mg, 0.04 mmol) and  $H_2SiF_6$  (100  $\mu$ L) were mixed in DMA(dimethylacetamide)/ $H_2O$ /EtOH (1:1:1, 3 mL) in a 10 mL glass container and tightly capped with a Teflon vial and heated at 95  $^{\circ}C$  for 48 h. After cooling to room temperature, the resulting blue-green crystals were harvested and washed with fresh DMA three times. Yield is  $\sim 49\%$  (based on the ligand).

**Synthesis of NTU-72.** **HL** (4 mg, 0.015 mmol),  $Cu(BF_4)_2$  (80 mg, 0.29 mmol),  $(NH_4)_2TiF_6$  (10 mg, 0.05 mmol) and  $H_2TiF_6$  (100  $\mu$ L) were mixed in DMA/ $H_2O$ /EtOH (1:1.5:1, 3.5 mL) in a 10 mL glass container and tightly capped with a Teflon vial and heated at 95  $^{\circ}C$  for 48 h. After cooling to room temperature, the resulting blue-green crystals were harvested and washed

with fresh DMA three times. Yield is  $\sim 53\%$  (based on the ligand).

**Synthesis of NTU-73.** **HL** (4 mg, 0.015 mmol),  $Cu(BF_4)_2$  (80 mg, 0.29 mmol),  $(NH_4)_2ZrF_6$  (10 mg, 0.04 mmol) and  $H_2ZrF_6$  (100  $\mu$ L) were mixed in DMA/ $H_2O$ /EtOH (1:1:1, 3 mL) in a 10 mL glass container and tightly capped with a Teflon vial and heated at 90  $^{\circ}C$  for 48 h. After cooling to room temperature, the resulting blue-green crystals were harvested and washed with fresh DMA three times. Yield is  $\sim 32\%$  (based on ligand).

## Results and discussion

### Synthesis and structure characterization

A reaction of copper(II) fluorosilicate with **HL** afforded polyhedron-shaped crystals (**NTU-71**). It crystallizes in a tetragonal  $I4_122$  space group with the formula of  $[Cu(HL)_2SiF_6] \cdot xguest$  (Table S1†). Its asymmetric unit includes one ligand, half a  $Cu^{2+}$  ion and half a  $SiF_6^{2-}$  ion (Fig. S1†). The charge of all the  $Cu^{2+}$  ions in **NTU-71** is balanced by  $SiF_6^{2-}$  ions, and thus, all the **HL** ligands are neutral. The single Cu node here is coordinated by four imidazole nitrogen atoms from four independent **HL** and two F atoms from two  $SiF_6^{2-}$  anions. Meanwhile, the three general branching points of the ligand take part in the coordination with the Cu nodes by two imidazole N atoms, while the carboxylate sites are free. As a third component of this framework, two F atoms from the  $SiF_6^{2-}$  anion join the coordination of the adjacent Cu node, yielding two helical chains in this 3D framework (Fig. S2†). Obviously, two channels with densely incorporated carboxylic groups can be observed along the  $b$ - and  $c$ -axis (Fig. 1a and S3 and S4†). Like crab pincers, these carboxylate groups are packed in pairs throughout the whole

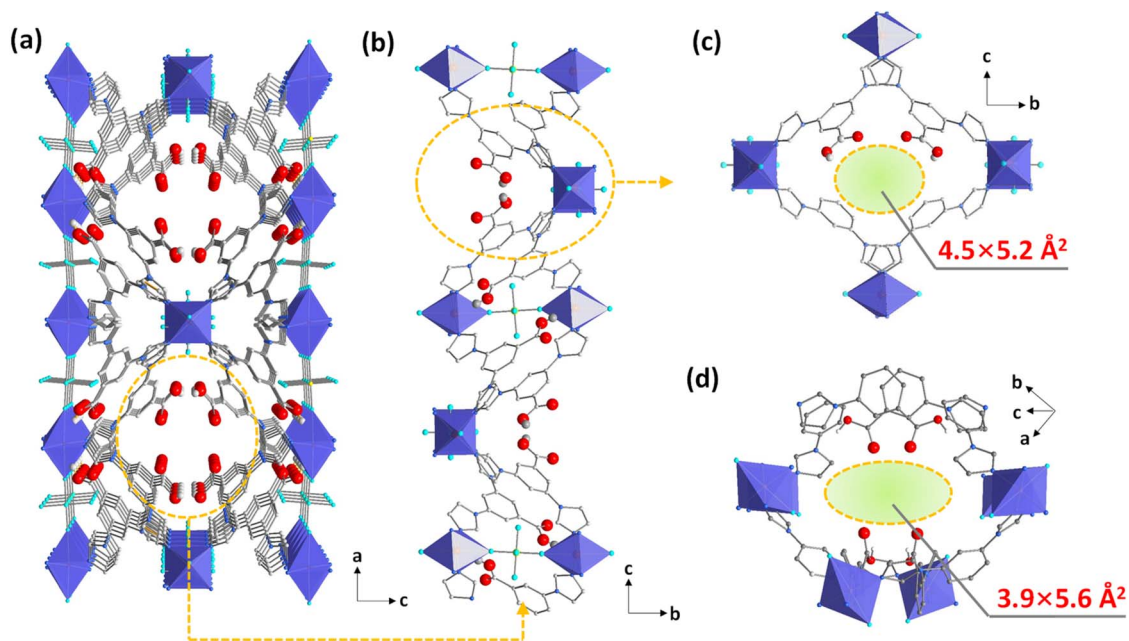


Fig. 1 Structure of **NTU-71**: view of the 1D channel that features carboxylic pincers along the  $b$ -axis (a); view of the pincers arranged alternately along the  $a$ -axis (b); local view of the nanospace defined by carboxylic pincers (c and d). Color codes: C, grey; N, blue; F, cyan; Si, yellow; O, red. The blue red polyhedron represents an octahedral coordinated Cu atom.



structure, and thus form a defined nanospace of about  $4.5 \times 5.2 \text{ \AA}^2$  (Fig. 1b and c). In addition, these carboxylic pincers are also available in another semiregular channel with an aperture size of  $3.9 \times 5.6 \text{ \AA}^2$  (Fig. 1d). To understand this structure better, topology analysis was performed.  $\text{Cu}(\text{HL})_2$  is an interpenetrated framework, of which each net can be simplified as a classical **dia** topology. Interestingly, these interpenetrated **dia** nets are then bridged by a 2-connected  $\text{SiF}_6^{2-}$  anion, yielding a new 6-c topology with a point symbol of  $\{4^8.6^7\}$  (Fig. S5†).

### Nanospace tuning

Encouraged by this structure and reticular chemistry,<sup>30</sup> the fine pore size engineering of the carboxylic-functionalized MOFs was performed, in which the balancing  $\text{SiF}_6^{2-}$  ions were replaced by  $\text{TiF}_6^{2-}$  and  $\text{ZrF}_6^{2-}$ , respectively. With a general formula of  $[\text{Cu}(\text{HL})_2\text{MF}_6]$ , the other two iso-reticular MOFs ( $M = \text{Ti}^{2+}$  and  $\text{Zr}^{2+}$ , termed **NTU-72** and **NTU-73**) were obtained (Fig. S6–S8†). Compared with that of **NTU-71** ( $d_{\text{O}\cdots\text{O}}$ : 5.021 Å), the pincer distance increased to 5.583 Å and 5.911 Å in **NTU-72** and **NTU-73**, respectively (Fig. 2). These fine changes may offer a fitted nanospace for carboxylic pincers to recognize  $\text{C}_2\text{H}_2$  clusters. The phase purity of these MOFs was examined by powder X-ray diffraction (PXRD). The diffraction peaks of the as-synthesized **NTU-series** are in good agreement with the simulated patterns, as well as the activated phases (Fig. S9–S11†).

### Pore evaluation

Permanent porosity of **NTU-71** to **NTU-73** was further explored by  $\text{N}_2$  (77 K) and  $\text{CO}_2$  (195 K and 298 K) adsorption measurements. They all display negligible  $\text{N}_2$  uptakes, but rapid and reversible type-I  $\text{CO}_2$  adsorptions, indicating typical microporous characteristics. Their maximum  $\text{CO}_2$  uptakes are 77, 82 and 71  $\text{cm}^3 \text{ cm}^{-3}$ , respectively (Fig. 3a). Their calculated BET surface areas (based on  $\text{CO}_2$ , 195 K) reach 242, 315 and 225  $\text{m}^2$

$\text{g}^{-1}$ , respectively, while the analysis of pore size distributions illustrate the systematic change of the nanospace (inset of Fig. 3a).

### Static adsorption selectivity and isosteric heats

Single-component adsorption isotherms of  $\text{C}_2\text{H}_2$  and  $\text{C}_2\text{H}_4$  were collected (Fig. 3b and S16–S21†), respectively. At 298 K, they all show relatively higher  $\text{C}_2\text{H}_2$  uptakes compared with  $\text{C}_2\text{H}_4$ . Interestingly, the  $\text{C}_2\text{H}_2$  uptakes ( $10.6 \text{ cm}^3 \text{ g}^{-1}$  and  $8.2 \text{ cm}^3 \text{ g}^{-1}$ ) at 1 kPa are almost 13–14 times higher than that of  $\text{C}_2\text{H}_4$  ( $0.8 \text{ cm}^3 \text{ g}^{-1}$  and  $0.6 \text{ cm}^3 \text{ g}^{-1}$ ) in **NTU-71** and **NTU-73**, and this ratio ( $15.8 \text{ cm}^3 \text{ g}^{-1}$  vs.  $1.0 \text{ cm}^3 \text{ g}^{-1}$ ) increases to 16 in **NTU-72** (Fig. S22†). These higher uptake ratios reflect preferred affinity of the three frameworks toward  $\text{C}_2\text{H}_2$  over  $\text{C}_2\text{H}_4$ . The adsorption selectivity of  $\text{C}_2\text{H}_2/\text{C}_2\text{H}_4$  (v/v, 1/99) in these three MOFs was predicted by ideal adsorbed solution theory (IAST) (Fig. 3c and S23–S35†).<sup>31,32</sup> The low-pressure  $\text{C}_2\text{H}_2$  adsorption selectivity of **NTU-72** ( $\sim 441$ ) is much higher than that of both **NTU-71** ( $\sim 58$ ) and **NTU-73** ( $\sim 147$ ), and is also higher than that of ZUL-200 (60),<sup>33</sup> **NTU-69** (49),<sup>34</sup> SIFSIX-2-Cu-i (45),<sup>7</sup> and JCM-1 (9).<sup>35</sup> In addition, the  $\text{C}_2\text{H}_2$  adsorption selectivities remain as high as 26, 56 and 38 at 1 bar. Particularly, the selectivity of **NTU-72** is only surpassed by the benchmark UTSA-200 (6320),<sup>36</sup> ZU-33 (1100),<sup>37</sup> and ZUL-series (175 and 114),<sup>33</sup> and is higher than most of the well known MOFs.<sup>7,38</sup>

To explore the reason for such high selectivities, isosteric heats of adsorption ( $Q_{\text{st}}$ ) of  $\text{C}_2\text{H}_2$  and  $\text{C}_2\text{H}_4$  were calculated (Fig. 3d and S36–S41†). The  $Q_{\text{st}}$  values of  $\text{C}_2\text{H}_4$  at low pressure (36.8, 36.7 and 35.7  $\text{kJ mol}^{-1}$ ) are all lower than that of  $\text{C}_2\text{H}_2$  (42.4, 43.5, and 40.9  $\text{kJ mol}^{-1}$ ) for the **NTU-series**. Similar to the higher  $\text{C}_2\text{H}_2$  uptake, the adsorption enthalpy difference of **NTU-72** (6.7  $\text{kJ mol}^{-1}$ ) is higher than that of **NTU-71** (5.6  $\text{kJ mol}^{-1}$ ) and **NTU-73** (5.2  $\text{kJ mol}^{-1}$ ). This may be due to the fine fitting of the pore geometry and size in **NTU-72** to the  $\text{C}_2\text{H}_2$  molecule,

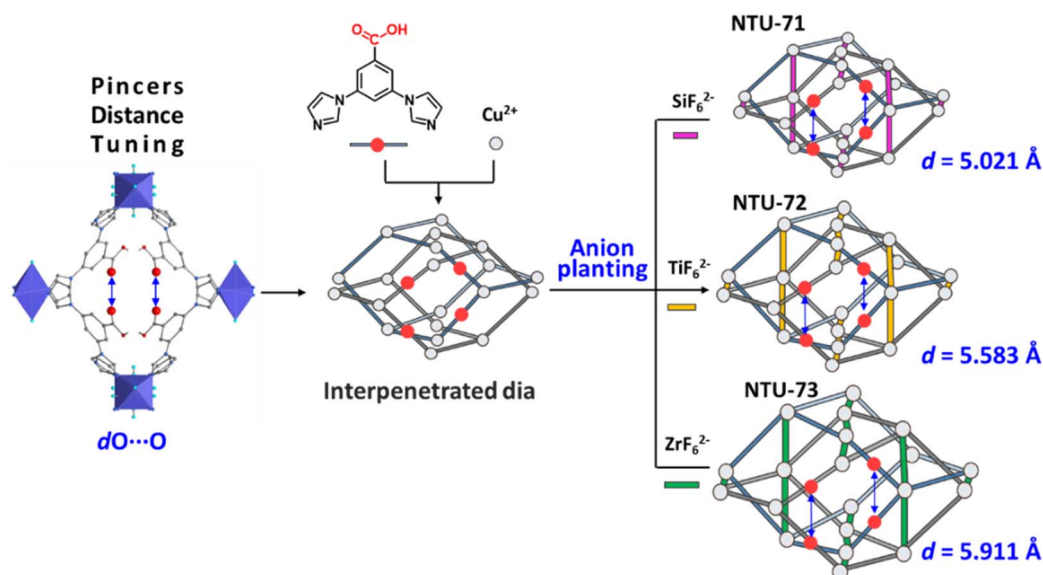


Fig. 2 Fine distance tuning in **NTU-series** via the anion planting approach, where  $d_{\text{O}\cdots\text{O}}$  increases at the sub-angstrom level.



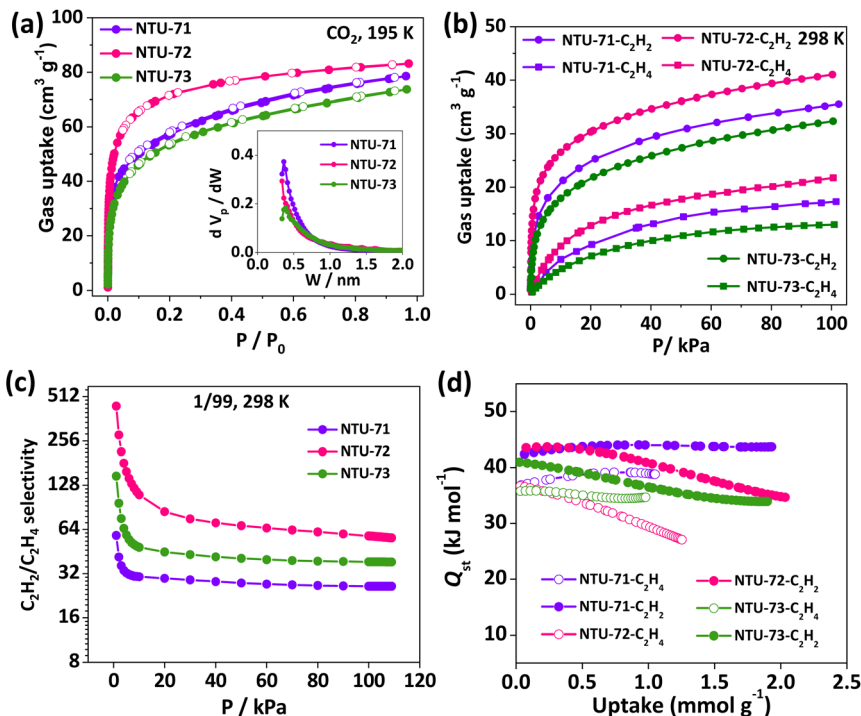


Fig. 3 Pore evaluation of the NTU-series:  $\text{CO}_2$  adsorption isotherms (a), inset is the pore size distribution;  $\text{C}_2\text{H}_2$  and  $\text{C}_2\text{H}_4$  isotherms (b); IAST selectivity (c); isosteric heats (d).

while the relatively larger or smaller nanospace in NTU-71 or NTU-73 provides a small interaction difference.

Breakthrough experiments were performed on NTU-72, in which the binary mixtures of  $\text{C}_2\text{H}_2/\text{C}_2\text{H}_4$  (v/v, 1/99) were introduced into the system. Pure  $\text{C}_2\text{H}_4$  passed through the sample bed as the first component ( $4.2 \text{ min g}^{-1}$ ), while  $\text{C}_2\text{H}_2$  is retained in the column (Fig. 4a). The mixtures of  $\text{C}_2\text{H}_2$  and  $\text{C}_2\text{H}_4$  were detected at about  $71.1 \text{ min g}^{-1}$ . This result shows that highly pure  $\text{C}_2\text{H}_4$  (99.95%) can be directly collected in  $66.9 \text{ min g}^{-1}$  at the adsorption stage. According to the sample weight and gas velocity, NTU-72 could produce  $331.1 \text{ cm}^3$  (STP) per g of pure  $\text{C}_2\text{H}_4$  from this mixture. To confirm the selective adsorption, the saturated adsorbents were then swept by helium at 298 K until no signal was detected. Subsequently,  $\text{C}_2\text{H}_2$  was desorbed by rapid heating (up to 323 K), and its purity is approximately 99.36% (Fig. 4b and S42 and S43<sup>†</sup>). Therefore, as an emerging example, NTU-72 can deliver both highly pure  $\text{C}_2\text{H}_4$  and  $\text{C}_2\text{H}_2$  in one adsorption/desorption cycle, although the recovery of poly-grade  $\text{C}_2\text{H}_4$  has been widely reported (Table S2<sup>†</sup>). Structural stability was then confirmed by cycling breakthrough experiments, where nearly the same separation curves were displayed (Fig. 4c). Further experiments with varied gas velocity (2 and  $10 \text{ cm}^3 \text{ min}^{-1}$ ) also showed obvious separation, and the  $\text{C}_2\text{H}_4$  productivity ( $319.6$  and  $323.8 \text{ cm}^3$  (STP) per g) has hardly suffered any impact (Fig. 4d and S44<sup>†</sup>).

To gain better understanding of the separation performance,  $\text{C}_2\text{H}_2$ - and  $\text{C}_2\text{H}_4$ -loaded NTU-72 crystals were investigated at 298 K.<sup>39</sup> As expected, both gases interact with the carboxylic sites (Fig. S45 and S46<sup>†</sup>). For  $\text{NTU-72} \supset \text{C}_2\text{H}_2$ , the occupancy of  $\text{C}_2\text{H}_2$  was refined to be 1, which corresponds to  $30.5 \text{ cm}^3 \text{ g}^{-1}$ , slightly

lower than the amount in the  $\text{C}_2\text{H}_2$  adsorption experiment ( $41 \text{ cm}^3 \text{ g}^{-1}$ ) at 1 bar. This difference may be caused by two reasons: (1) the  $\text{C}_2\text{H}_2$  molecules at other free space are strongly disordered and hard to be accurately modelled; (2) part of the  $\text{C}_2\text{H}_2$  escaped during the sealing of the glass tube by using a hot candle. Despite this, the position and geometry of the adsorbed  $\text{C}_2\text{H}_2$  molecules can be clearly identified in this confined nanospace. The  $\text{C}_2\text{H}_2$  molecules are confined in the channel through three types of hydrogen bonds in different binding geometries (Fig. 5a and b). Acting as an acceptor and a donor, the  $\text{O}_{\text{COOH}}$  and  $\text{OH}_{\text{COOH}}$  moieties connect the terminal hydrogen and carbon atoms of a  $\text{C}_2\text{H}_2$  molecule. In addition, the  $\text{OH}_{\text{COOH}}$  moiety also forms a hydrogen bond with another  $\text{C}_2\text{H}_2$  molecule, resulting in close packing of the two gas molecules with intermolecular hydrogen bonds. Meanwhile, the terminal  $\text{H}_{\text{C}_2\text{H}_2}$  forms hydrogen bonds with  $\text{C}_{\text{C}_2\text{H}_2}$  from its symmetrically equivalent molecule, so that a  $\text{C}_2\text{H}_2$  tetramer with  $C_{2h}$  symmetry is formed periodically in NTU-72 (Fig. S47–S49<sup>†</sup>), which is different from the  $S_4$  symmetric  $\text{C}_2\text{H}_2$  tetramer in SIFSIX-Cu-*i*.<sup>7</sup> Although the  $\text{C}_2\text{H}_2$  clusters have been investigated,<sup>20,21</sup> a compact  $\text{C}_2\text{H}_2$  tetramer with  $C_{2h}$  symmetry being stabilized by chelating carboxylic pincers is found for the first time. Sharply in contrast, two types of hydrogen bonds are observed in  $\text{NTU-72} \supset \text{C}_2\text{H}_4$  (Fig. 5c and d and S50–S52<sup>†</sup>). Particularly,  $d_{\text{C}_2\text{H}_4 \cdots \text{H}-\text{O}_{\text{COOH}}}$  ( $2.705 \text{ \AA}$ ) is much longer than that of  $d_{\text{C}_2\text{H}_2 \cdots \text{H}-\text{O}_{\text{COOH}}}$  ( $1.871$  and  $2.588 \text{ \AA}$ ), as well as the longer  $d_{\text{O}_{\text{COOH}} \cdots \text{H}-\text{O}_{\text{C}_2\text{H}_4}}$ , reflecting relative weak carboxylic- $\text{C}_2\text{H}_4$  interaction. Furthermore, no intermolecular interaction is found between the two  $\text{C}_2\text{H}_4$  molecules, as their distance is far. Therefore, the carboxylic sites contribute mainly to the



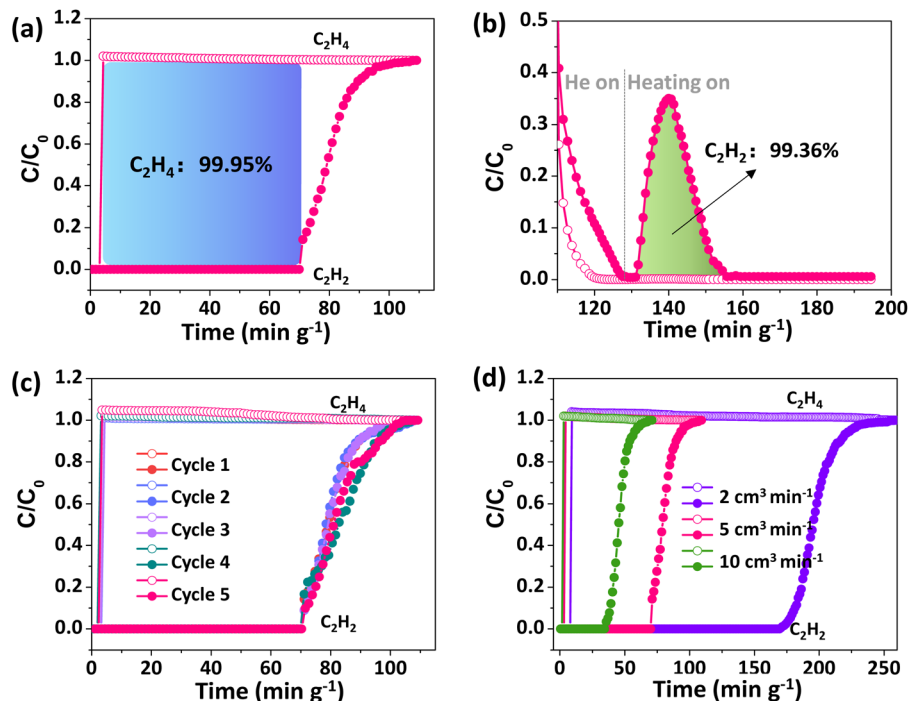


Fig. 4 Breakthrough curves of NTU-72 for a  $C_2H_2/C_2H_4$  mixture (1/99, v/v) at 298 K, 1 bar, velocity is  $5\text{ cm}^3\text{ min}^{-1}$  (a); desorption curves (b); cycle breakthrough tests (c); (d) breakthrough curves at different velocities.

recognition of the  $C_2H_2$  tetramer, and meanwhile, the finely engineered pore geometry and nano-size confined this cluster to be released in the pure form. Further Raman spectra of gas loaded NTU-72 show that the peak at  $1950\text{ cm}^{-1}$  belonging to the tensile vibration of  $C_2H_2$  was found in NTU-72, and in contrast, no helium peak was found (Fig. 5e).<sup>40,41</sup> In addition,

the corresponding peak that belongs to  $C_2H_4$  (theoretical position:  $1689\text{ cm}^{-1}$ ) can't be observed. Therefore, it is rational to conclude that the  $C_2H_2$  clusters assembled in a periodic configuration in NTU-72, agreeing well with the crystallographic studies.

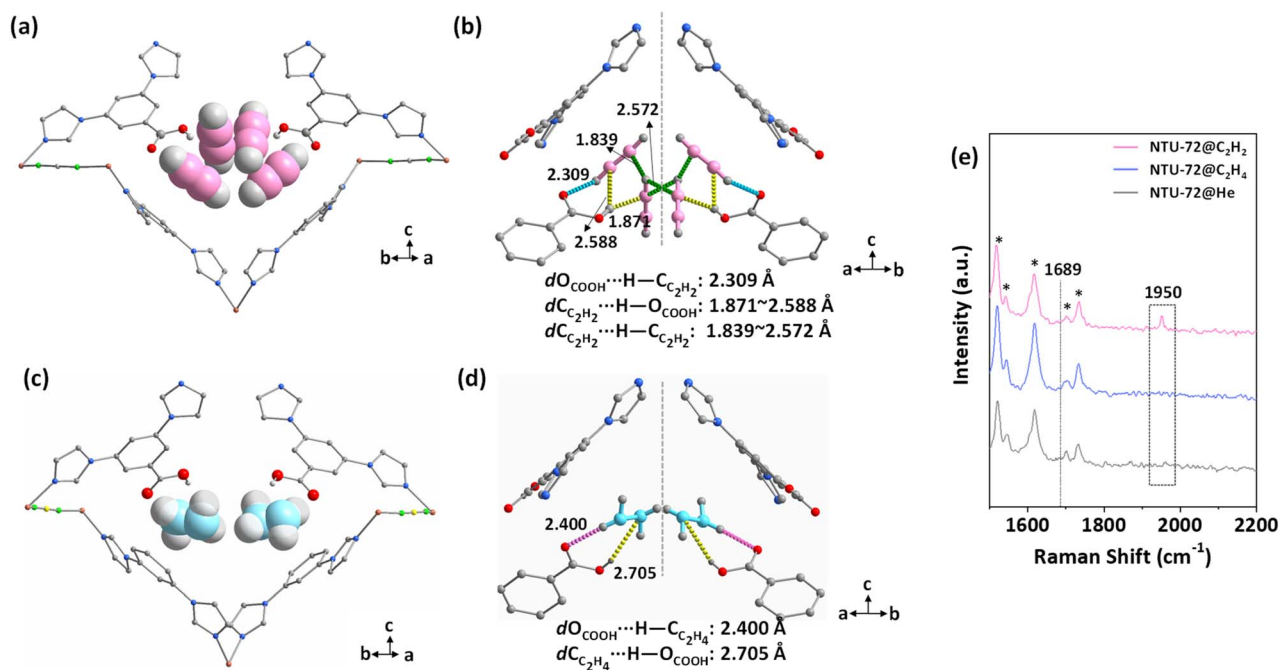


Fig. 5 Structure of  $C_2H_2$ - (a and b) and  $C_2H_4$ - (c and d) loaded NTU-72. Raman spectra of gas-loaded NTU-72 (e).



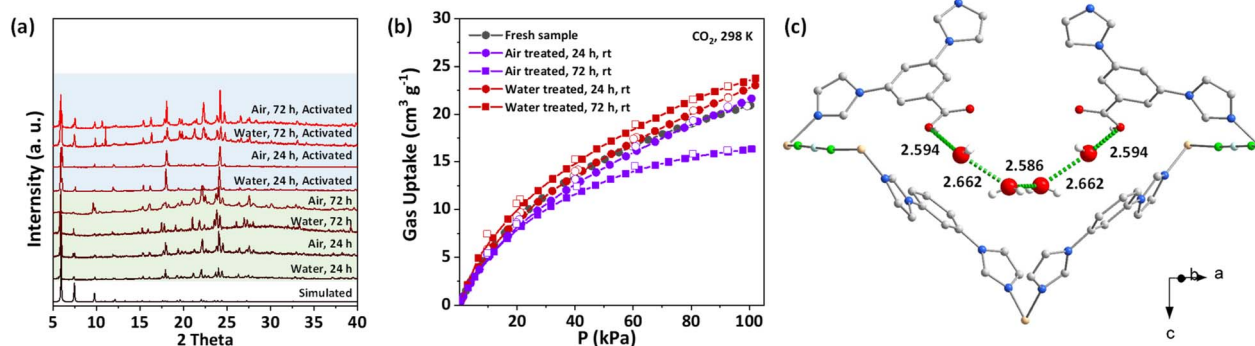


Fig. 6 PXR D (a) and CO<sub>2</sub> adsorption isotherms (b) of water and moisture treated NTU-72; local view of the structure of NTU-72·H<sub>2</sub>O (c), and the unit of O...O distance is Å.

### Stability

The water/air stability of NTU-72 was then evaluated at room temperature. As shown in Fig. S53,† NTU-72 retained a polyhedral shape after air treatment, but some changes occurred in the shape after water treatment. Single crystal X-ray analysis showed that the water treated crystal (NTU-72·H<sub>2</sub>O, for 72 h) retains the framework of the as-synthesized phase (Table S1†), confirmed further by PXR D analysis. Additionally, adsorption measurements revealed that the CO<sub>2</sub> capacity of all treated samples is consistent with that of fresh samples, except for a slight decrease in the air treated sample for 72 h. These results confirm that NTU-72 has good water and moisture robustness (Fig. 6a and b). Considering the structure, the maintained crystallinity of NTU-72 is due to the relatively strong Cu–N bond, similar to that of NTU-67, having a highly robust framework with a Cu–N coordination sphere also.<sup>39</sup> In addition, the crystal structure of NTU-72·H<sub>2</sub>O shows that a couple of carboxylic pincers bind a tetra-water cluster *via* short hydrogen bonds ( $d_{O...O}$ : 2.586–2.662 Å), which may provide a blocking effect for other water molecules to reach the coordination bonds (Fig. 6c).

### Conclusions

In conclusion, as needed for the pure C<sub>2</sub> hydrocarbons, we have finely tuned a new family of carboxylic-functionalized MOFs and afforded NTU-72 with high adsorption C<sub>2</sub>H<sub>2</sub>/C<sub>2</sub>H<sub>4</sub> selectivity as well as unprecedented recovery of highly pure C<sub>2</sub>H<sub>4</sub> and C<sub>2</sub>H<sub>2</sub>. The carboxylic pincers contribute to the recognition of a C<sub>2</sub>H<sub>2</sub> tetramer, and the fitted pore geometry/size enforces synergistic binding and restricts this cluster to be released in a pure form. In addition, this material is stable in water and moisture environments. The foregoing results not only present an excellent MOF for energy-saving C<sub>2</sub> hydrocarbon purification, but also provide a novel approach for the selective binding of gas clusters for designing advanced MOFs.

### Data availability

All data can be found in the main text and ESI.†

### Author contributions

J. D. conceived the idea of this work. Y. D. and Y. H. carried out the experiments and analyzed the results. J. D. and J. B. wrote the paper. C. W. performed the repeated adsorption experiments. H. W. prepared the ligands. All authors gave valuable discussion and suggestion for the final draft.

### Conflicts of interest

The authors declare no competing interests.

### Acknowledgements

We are thankful for the financial support of the National Natural Science Foundation of China (22171135 and 22271150), the Young and Middle-aged Academic Leader of Jiangsu Provincial Blue Project, the State Key Laboratory of Materials-Oriented Chemical Engineering (ZK201803) and Open Foundation of Hunan Provincial Key Laboratory of Controllable Preparation and Functional Application of Fine Polymers (E22306).

### References

- 1 D. S. Sholl and R. P. Lively, *Nature*, 2016, **532**, 435–437.
- 2 R. Matsuda, R. Kitaura, S. Kitagawa, Y. Kubota, R. V. Belosludov, T. C. Kobayashi, H. Sakamoto, T. Chiba, M. Takata, Y. Kawazoe and Y. Mita, *Nature*, 2005, **436**, 238–241.
- 3 Y. Chai, X. Han, W. Li, S. Liu, S. Yao, C. Wang, W. Shi, I. da-Silva, P. Manuel, Y. Cheng, L. D. Daemen, A. J. Ramirez-Cuesta, C. C. Tang, L. Jiang, S. Yang, N. Guan and L. Li, *Science*, 2020, **368**, 1002–1006.
- 4 K. J. Chen, D. G. Madden, S. Mukherjee, T. Pham, K. A. Forrest, A. Kumar, B. Space, J. Kong, Q. Y. Zhang and M. J. Zaworotko, *Science*, 2019, **366**, 241–246.
- 5 F. Studt, F. Abild-Pedersen, T. Bligaard, R. Z. Sorensen, C. H. Christensen and J. K. Norskov, *Science*, 2008, **320**, 1320–1322.



- 6 E. D. Bloch, W. L. Queen, R. Krishna, J. M. Zadrozny, C. M. Brown and J. R. Long, *Science*, 2012, **335**, 1606–1610.
- 7 X. L. Cui, K. J. Chen, H. B. Xing, Q. W. Yang, R. Krishna, Z. B. Bao, H. Wu, W. Zhou, X. L. Dong, Y. Han, B. Li, Q. L. Ren, M. J. Zaworotko and B. L. Chen, *Science*, 2016, **353**, 141–144.
- 8 B. Li, X. Cui, D. O’Nolan, H. M. Wen, M. Jiang, R. Krishna, H. Wu, R. B. Lin, Y. S. Chen, D. Yuan, H. Xing, W. Zhou, Q. Ren, G. Qian, M. J. Zaworotko and B. Chen, *Adv. Mater.*, 2017, **29**, 1704210–1704217.
- 9 H. Zeng, M. Xie, T. Wang, R. J. Wei, X. J. Xie, Y. F. Zhao, W. G. Lu and D. Li, *Nature*, 2021, **595**, 542–548.
- 10 A. Cadiou, K. Adil, P. M. Bhatt, Y. Belmabkhout and M. Eddaoudi, *Science*, 2016, **353**, 137–140.
- 11 Q. Dong, Y. Huang, J. Wan, Z. Lu, Z. Wang, C. Gu, J. Duan and J. Bai, *J. Am. Chem. Soc.*, 2023, DOI: [10.1021/jacs.3c00515](https://doi.org/10.1021/jacs.3c00515).
- 12 H. Li, M. Eddaoudi, M. O’Keeffe and O. M. Yaghi, *Nature*, 1999, **402**, 276–279.
- 13 S. Krause, V. Bon, I. Senkovska, U. Stoeck, D. Wallacher, D. M. Tobbens, S. Zander, R. S. Pillai, G. Maurin, F. X. Coudert and S. Kaskel, *Nature*, 2016, **532**, 348–352.
- 14 S. H. Lo, L. Feng, K. Tan, Z. H. Huang, S. Yuan, K. Y. Wang, B. H. Li, W. L. Liu, G. S. Day, S. S. Tao, C. C. Yang, T. T. Luo, C. H. Lin, S. L. Wang, S. J. L. Billinge, K. L. Lu, Y. J. Chabal, X. D. Zou and H. C. Zhou, *Nat. Chem.*, 2020, **12**, 90–97.
- 15 H. Wang, X. L. Dong, V. Colombo, Q. N. Wang, Y. Y. Liu, W. Liu, X. L. Wang, X. Y. Huang, D. M. Proserpio, A. Sironi, Y. Han and J. Li, *Adv. Mater.*, 2018, **30**, 1805088–1805096.
- 16 Y. L. Peng, T. Pham, P. Li, T. Wang, Y. Chen, K. J. Chen, K. A. Forrest, B. Space, P. Cheng, M. J. Zaworotko and Z. Zhang, *Angew. Chem., Int. Ed.*, 2018, **57**, 10971–10975.
- 17 R. B. Lin, L. B. Li, H. Wu, H. Arman, B. Li, R. G. Lin, W. Zhou and B. L. Chen, *J. Am. Chem. Soc.*, 2017, **139**, 8022–8028.
- 18 J. P. Zhang, P. Q. Liao, H. L. Zhou, R. B. Lin and X. M. Chen, *Chem. Soc. Rev.*, 2014, **43**, 5789–5814.
- 19 N. Behera, J. Duan, W. Jin and S. Kitagawa, *EnergyChem*, 2021, **3**, 100067–100124.
- 20 K. Shuler and C. E. Dykstra, *J. Phys. Chem. A*, 2000, **104**, 11522–11530.
- 21 J. G. Yu, S. J. Su and J. E. Bloor, *J. Phys. Chem.*, 1990, **94**, 5589–5592.
- 22 R. Custelcean and M. G. Gorbunova, *J. Am. Chem. Soc.*, 2005, **127**, 16362–16363.
- 23 X. Duan, R. J. Song, J. C. Yu, H. L. Wang, Y. J. Cui, Y. Yang, B. L. Chen and G. D. Qian, *RSC Adv.*, 2014, **4**, 36419–36424.
- 24 F. Ragon, B. Campo, Q. Yang, C. Martineau, A. D. Wiersum, A. Lago, V. Guillerm, C. Hemsley, J. F. Eubank, M. Vishnuvarthan, F. Taulelle, P. Horcajada, A. Vimont, P. L. Llewellyn, M. Daturi, S. Devautour-Vinot, G. Maurin, C. Serre, T. Devic and G. Clet, *J. Mater. Chem. A*, 2015, **3**, 3294–3309.
- 25 J. Duan, M. Higuchi, J. Zheng, S. I. Noro, I. Y. Chang, K. Hyeon-Deuk, S. Mathew, S. Kusaka, E. Sivaniah, R. Matsuda, S. Sakaki and S. Kitagawa, *J. Am. Chem. Soc.*, 2017, **139**, 11576–11583.
- 26 Z. Y. Lu, L. T. Du, R. Y. Guo, G. B. Zhang, J. G. Duan, J. F. Zhang, L. Han, J. F. Bai and J. T. Hupp, *J. Am. Chem. Soc.*, 2021, **143**, 17942–17946.
- 27 M. X. Zhang, W. Zhou, T. Pham, K. A. Forrest, W. L. Liu, Y. B. He, H. Wu, T. Yildirim, B. L. Chen, B. Space, Y. Pan, M. J. Zaworotko and J. F. Bai, *Angew. Chem., Int. Ed.*, 2017, **56**, 11426–11430.
- 28 L. Du, Z. Lu, K. Zheng, J. Wang, X. Zheng, Y. Pan, X. You and J. Bai, *J. Am. Chem. Soc.*, 2013, **135**, 562–565.
- 29 M. Li, D. Li, M. O’Keeffe and O. M. Yaghi, *Chem. Rev.*, 2014, **114**, 1343–1370.
- 30 N. W. Ockwig, O. Delgado-Friedrichs, M. O’Keeffe and O. M. Yaghi, *Acc. Chem. Res.*, 2005, **38**, 176–182.
- 31 J. G. Duan, M. Higuchi, S. Horike, M. L. Foo, K. P. Rao, Y. Inubushi, T. Fukushima and S. Kitagawa, *Adv. Funct. Mater.*, 2013, **23**, 3525–3530.
- 32 R. Krishna, *RSC Adv.*, 2015, **5**, 52269–52295.
- 33 J. Shen, X. He, T. Ke, R. Krishna, J. M. van Baten, R. Chen, Z. Bao, H. Xing, M. Dinca, Z. Zhang, Q. Yang and Q. Ren, *Nat. Commun.*, 2020, **11**, 6259.
- 34 Y. Huang, Y. Xu, B. Zheng, Z. Wang, Q. Dong and J. Duan, *Energy Fuels*, 2020, **34**, 11315–11321.
- 35 J. Lee, C. Y. Chuah, J. Kim, Y. Kim, N. Ko, Y. Seo, K. Kim, T. H. Bae and E. Lee, *Angew. Chem., Int. Ed.*, 2018, **57**, 7869–7873.
- 36 H. Li, L. Li, R. B. Lin, G. Ramirez, W. Zhou, R. Krishna, Z. Zhang, S. Xiang and B. Chen, *ACS Sustainable Chem. Eng.*, 2019, **7**, 4897–4902.
- 37 Z. Zhang, X. Cui, L. Yang, J. Cui, Z. Bao, Q. Yang and H. Xing, *Ind. Eng. Chem. Res.*, 2018, **57**, 7266–7274.
- 38 J. Wang, L. Li, L. Guo, Y. Zhao, D. Xie, Z. Zhang, Q. Yang, Y. Yang, Z. Bao and Q. Ren, *Chem.–Eur. J.*, 2019, **25**, 15516–15524.
- 39 Q. B. Dong, Y. H. Huang, K. Hyeon-Deuk, I. Y. Chang, J. M. Wan, C. L. Chen, J. G. Duan, W. N. Jin and S. Kitagawa, *Adv. Funct. Mater.*, 2022, **32**, 2203745–2203755.
- 40 H. Wang, Y. Duan, Y. Wang, Y. Huang, K. Ge, S. Wang, B. Zheng, Z. Wang, J. Bai and J. Duan, *ACS Appl. Mater. Interfaces*, 2022, **14**, 13550–13559.
- 41 G. C. Guo, S. H. Lin, F. K. Zheng, Z. C. Dong and J. S. Huang, *Spectrosc. Spectral Anal.*, 2000, **20**, 830–832.

